Supplementary material for "Quantifying future Arctic and Antarctic climate change from a storyline perspective using global variable-resolution models"

Lise Seland Graff[1], Dörthe Handorf[2], Raphael Köhler[2], Xavier Levine[3,a], René R. Wijngaard[4], Ryan S. Williams[5], Gareth J. Marshall[5], and Priscilla A. Mooney[2]

[1]Norwegian Meteorological Institute, Oslo, Norway
[2]Alfred Wegener Institute, Helmholtz Centre for Polar and Marine Research, Potsdam, Germany
[3]NORCE Norwegian Research Centre AS and Bjerknes Centre for Climate Research, Bergen, Norway
[a]now at: Department of Earth and Environmental Sciences, Columbia University, New York, USA
[4]Utrecht University, Utrecht, the Netherlands
[5]British Antarctic Survey, Cambridge, UK

Correspondence: Lise Seland Graff (lise.s.graff@met.no)

1 Overview

This supplementary material contains additional tables and figures.

List of Tables

List of Figures

2 CMIP6 models used for Antarctic storylines

Table S1. Overview of CMIP6 models (column 1) used for the Antarctic storyline results in Fig. 1 and Table 3, the modeling centers (column 2), and data citations for the respective historical and SSP5-8.5 experiments (columns 3). The model selection is as in Williams et al. (2024).

CMIP6 model	**Modeling center**	**Data citations (historical & SSP5-8.5)**
ACCESS-CM2	CSIRO-ARCCSS	Dix et al. (2019a, b)
ACCESS-ESM1-5	CSIRO	Ziehn et al. (2019b, a)
BCC-CSM2-MR	BCC	Wu et al. (2018); Xin et al. (2019)
CAMS-CSM1-0	CAMS	Rong (2019a, b)
CAS-ESM2-0	CAS	Chai (2020); Chinese Academy Of Sciences (CAS) (2020)
CESM2	NCAR	Danabasoglu (2019a, b)
CESM2-WACCM	NCAR	Danabasoglu (2019c, d)
CIESM	THU	Huang (2019, 2020)
CMCC-CM2-SR5	CMCC	Lovato and Peano (2020b, a)
CMCC-ESM2	CMCC	Lovato et al. (2021b, a)
CNRM-CM6-1	CNRM-CERFACS	Voldoire (2018, 2019c)
CNRM-CM6-1-HR	CNRM-CERFACS	Voldoire (2019a, b)
CNRM-ESM2-1	CNRM-CERFACS	Seferian (2018); Voldoire (2019d)
E3SM-1-1	E3SM-Project	Bader et al. (2020a, b)
EC-Earth3	EC-Earth-Consortium	EC-Earth Consortium (EC-Earth) (2019c, d)
EC-Earth3-CC	EC-Earth-Consortium	EC-Earth Consortium (EC-Earth) (2021a, b)
EC-Earth3-Veg	EC-Earth-Consortium	EC-Earth Consortium (EC-Earth) (2019a, b)
EC-Earth3-Veg-LR	EC-Earth-Consortium	EC-Earth Consortium (EC-Earth) (2020a, b)
FIO-ESM2-0	FIO-QLNM	Song et al. (2019a, b)
GFDL-CM4	NOAA-GFLD	Guo et al. (2018a, b)
GFDL-ESM4	NOAA-GFLD	Krasting et al. (2018); John et al. (2018)
GISS-E2-1-G	NASA-GISS	NASA Goddard Institute For Space Studies (NASA/GISS) (2018, 2020)
HadGEM3-GC31-LL	MOHC	Ridley et al. (2019a); Good (2020)
HadGEM3-GC31-MM	MOHC	Ridley et al. (2019b); Jackson (2020)
INM-CM5-0	INM	Volodin et al. (2019a, b)
IPSL-CM6A-LR	IPSL	Boucher et al. (2018, 2019)
KIOST-ESM	KIOST	Kim et al. (2019a, b)
MPI-ESM1-2-HR	MPI-M & DKRZ	Jungclaus et al. (2019); Schupfner et al. (2019)
MPI-ESM1-2-LR	MPI-M	Wieners et al. (2019b, a)
MRI-ESM2-0	MRI	Yukimoto et al. (2019a, b)
NESM3	NUIST	Cao and Wang (2019); Cao (2019)
UKESM1-0-LL	MOHC	Tang et al. (2019); Good et al. (2019)

3 Definitions of future responses

Table S2. Overview of the full set of future responses for Arctic storyline models and VR-model experiments, computed as the difference between experiments for the future and relatively recent past. We list the names of the future responses in column 1, the category the model belongs to (CMIP6 or variable resolution [VR]) in column 2, the model name in column 3, and the future and past experiments in column 4–5, respectively. For the VR models, we list the storyline model from which the prescribed SST and SIC fields are derived in column 6. The storyline models are defined in Table 1 in the main text. Note that for the CMIP6 models, SSTs and SICs are computed by the models own ocean and sea-ice component. The time periods are given in the footnotes.

Response name	Category	Model	Future run	Recent-past run	SST & SIC
Arc-1 CNRM-10	CMIP6	CNRM	ssp585[1]	historical[2]	N/A
Arc-1 CNRM-30	CMIP6	CNRM	ssp585[3]	historical[4]	N/A
Arc-1 CESM-UU	VR	CESM	future unref[1]	recent-past unref[2]	CNRM
Arc-1 CESM-RU	VR	CESM	future dual-polar ref[1]	recent-past unref[2]	CNRM
Arc-1 ICON-UU	VR	ICON	future unref[1]	recent-past unref[2]	CNRM
Arc-1 ICON-RU	VR	ICON	future Arctic ref[1]	recent-past unref[2]	CNRM
Arc-1 MPAS-UU	VR	MPAS	future unref[1]	recent-past unref[2]	CNRM
Arc-1 MPAS-RU	VR	MPAS	future Arctic ref[1]	recent-past unref[2]	CNRM
Arc-2 NorESM-10	CMIP6	NorESM	ssp585[1]	historical[2]	N/A
Arc-2 NorESM-30	CMIP6	NorESM	ssp585[3]	historical[4]	N/A
Arc-2 CESM-UU	VR	CESM	future unref[1]	recent-past unref[2]	NorESM
Arc-2 CESM-RU	VR	CESM	future dual-polar ref[1]	recent-past unref[2]	NorESM
Arc-2 ICON-UU	VR	ICON	future unref[1]	recent-past unref[2]	NorESM
Arc-2 ICON-RU	VR	ICON	future Arctic ref[1]	recent-past unref[2]	NorESM
Arc-2 MPAS-UU	VR	MPAS	future unref[1]	recent-past unref[2]	NorESM
Arc-2 MPAS-RU	VR	MPAS	future Arctic ref[1]	recent-past unref[2]	NorESM

[1] 2090–2099; [2] 2005–2014; [3] 2070–2099; [4] 1985–2014; N/A, not applicable.

Table S3. As in Table S2, but for future responses for Antarctic storyline-model and VR-model experiments.

Response name	Category	Model	Future run	Recent-past run	SST & SIC
Ant-1 WACCM-10	CMIP6	WACCM	ssp585[1]	historical[2]	N/A
Ant-1 WACCM-30	CMIP6	WACCM	ssp585[3]	historical[4]	N/A
Ant-1 CESM-UU	VR	CESM	future unref[1]	recent-past unref[2]	WACCM
Ant-1 CESM-RU	VR	CESM	future dual-polar ref[1]	recent-past unref[2]	WACCM
Ant-1 ICON-UU	VR	ICON	future unref[1]	recent-past unref[2]	WACCM
Ant-1 ICON-RU	VR	ICON	future Antarctic ref[1]	recent-past unref[2]	WACCM
Ant-1 MPAS-UU	VR	MPAS	future unref[1]	recent-past unref[2]	WACCM
Ant-1 MPAS-RU	VR	MPAS	future Antarctic ref[1]	recent-past unref[2]	WACCM
Ant-2 MPI-10	CMIP6	MPI	ssp585[1]	historical[2]	N/A
Ant-2 MPI-30	CMIP6	MPI	ssp585[3]	historical[4]	N/A
Ant-2 CESM-UU	VR	CESM	future unref[1]	recent-past unref[2]	MPI
Ant-2 CESM-RU	VR	CESM	future dual-polar ref[1]	recent-past unref[2]	MPI
Ant-2 ICON-UU	VR	ICON	future unref[1]	recent-past unref[2]	MPI
Ant-2 ICON-RU	VR	ICON	future Antarctic ref[1]	recent-past unref[2]	MPI
Ant-2 MPAS-UU	VR	MPAS	future unref[1]	recent-past unref[2]	MPI
Ant-2 MPAS-RU	VR	MPAS	future Antarctic ref[1]	recent-past unref[2]	MPI

[1] 2090–2099; [2] 2005–2014; [3] 2070–2099; [4] 1985–2014; N/A, not applicable.

4 Plots for Antarctic storylines for sea-ice concentration

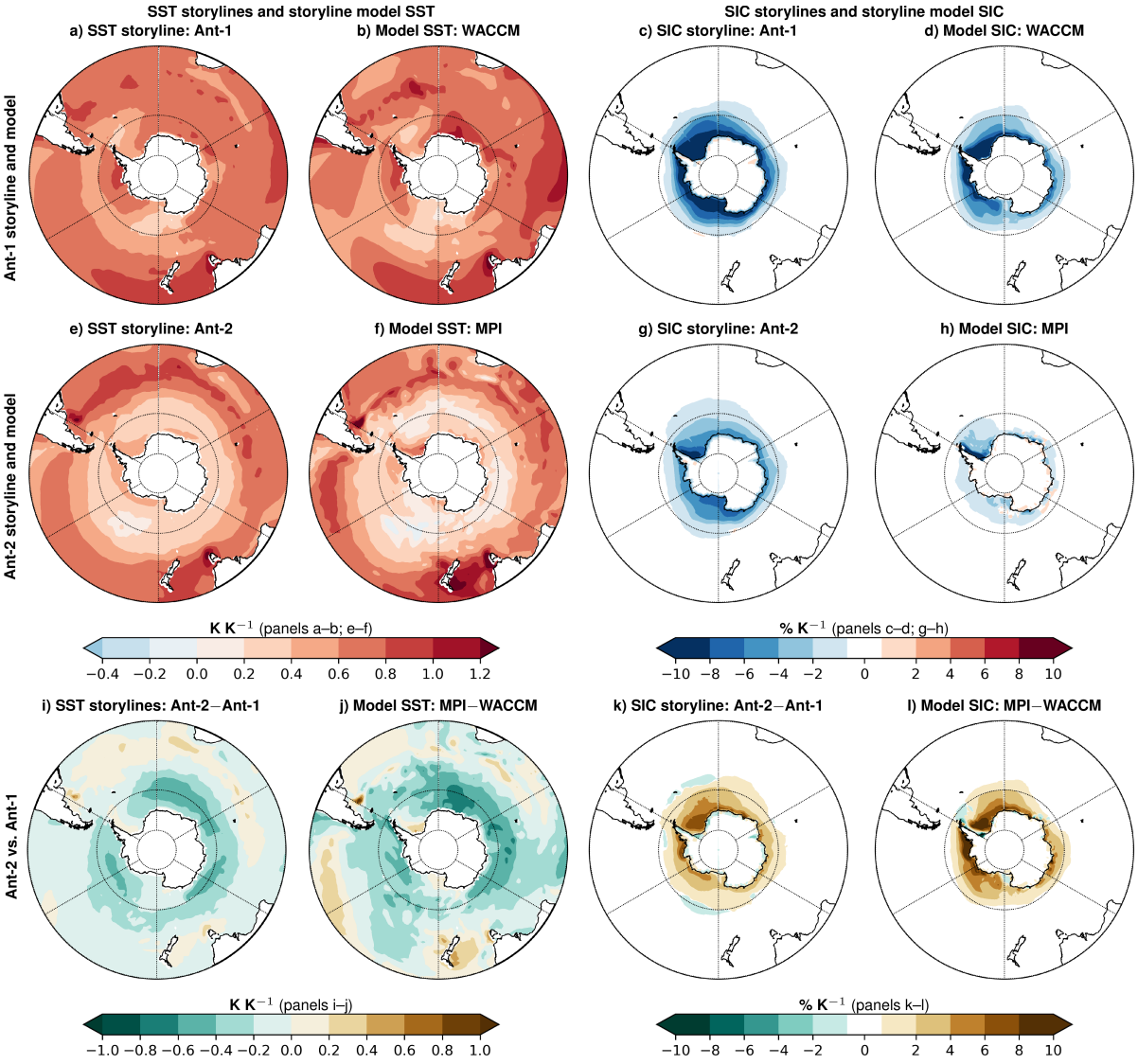

Figure S1. SST and SIC storylines for DJFM, derived using the framework from W24, shown with the SST and SIC fields from the storyline models (WACCM and MPI), and with the difference between the storylines (Ant-2 vs. Ant-1) and between the storyline models (MPI vs. WACCM) for 2070–2099−1985–2014. The top row shows the Ant-1 SST (a) and SIC (c) storylines with the SST (b) and SIC (d) field from the Ant-1 storyline model WACCM. The middle row shows (e–h) shows the same for Ant-2 and the Ant-2 storyline model MPI. The bottom row shows the difference Ant-2 and Ant-1 SST (i) and SIC (k) storylines with the difference between the SST (j) and SIC (l) fields from the Ant-2 and Ant-1 storyline models. The storylines are derived for the same CMIP6 models as in W24 (Table S1). The fields are scaled by global near-surface warming in line with W24. Units are K K^{-1} (a–b; e–f; i–j) and % K^{-1} (d–f; g–h; k–l).

5 Plots for Arctic storyline-model and VR-model experiments

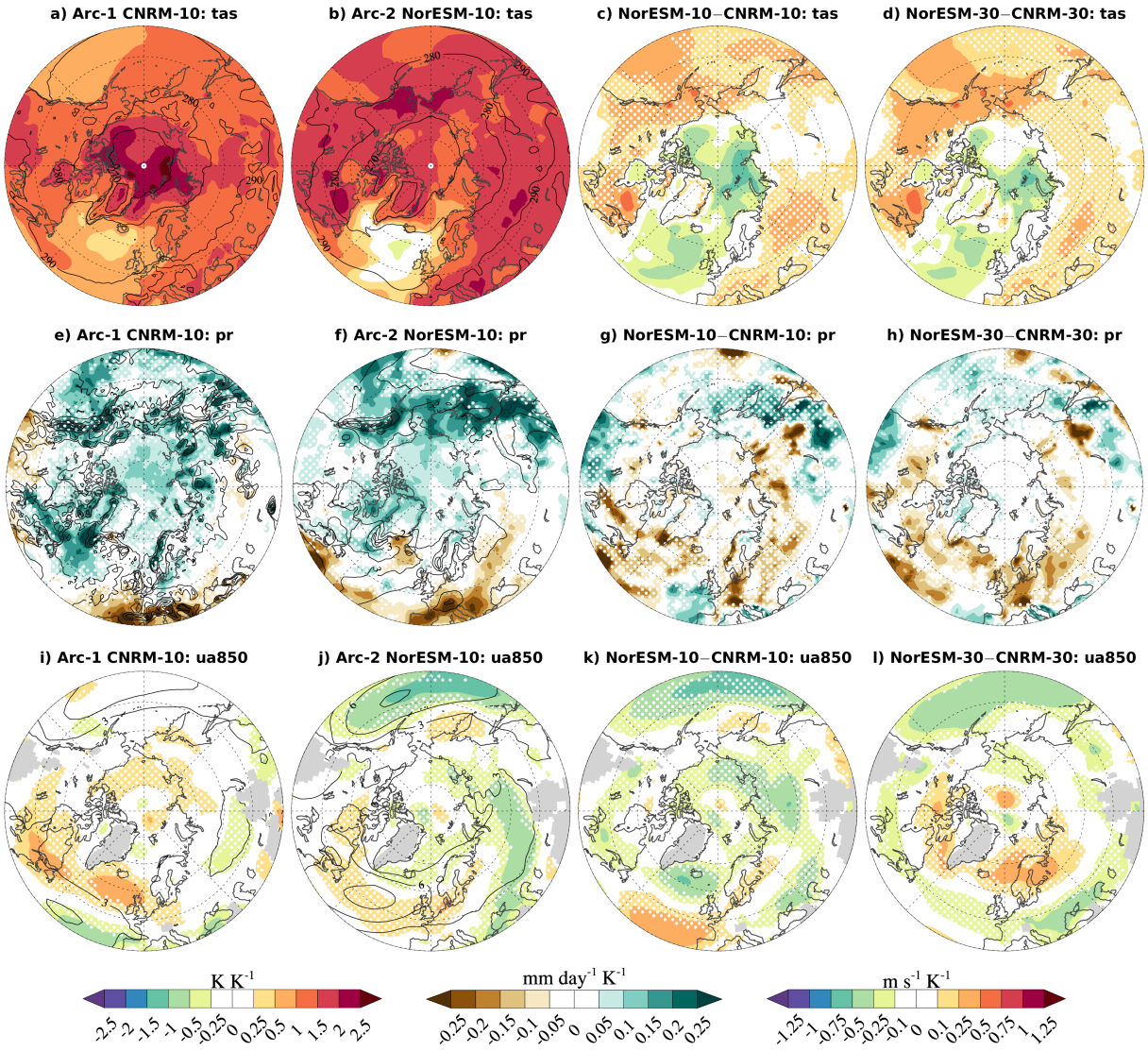

Figure S2. Future changes in near-surface temperature (tas; a–d), total precipitation rate (pr; e–h), and 850-hPa zonal wind (ua850; i–l) for the Arctic storyline models during MJJASO. We show the future response for Arc-1 CNRM-10 (a, e, and i) and Ant-2 NorESM-10 (b, f, and j). To highlight the difference between the storyline models and assess the sensitivity to the time periods, we also show the difference between Arc-2 NorESM-10 and Arc-1 CNRM-10 (that is, the difference between the future responses; c, g, and k), and between Arc-2 NorESM-30 and Arc-1 CNRM-30 (d, h, and l). The future responses are defined in Table S2. Black solid contours (a–b, e–f, and i–j) are climatology contours from the respective historical experiment for reference. White dots indicate changes that are *not significant* at the 95% level according to a two-sided T-test. The fields are normalized by the global near-surface warming of the respective experiments. Note that the responses in a–b, e–f, and i–j are also shown in Fig. 3 and Fig. 4 in the main text, but are repeated here for convenience. Units are K K^{-1} (a–d), mm day^{-1} K^{-1} (d–h), and m s^{-1} K^{-1} (i–l).

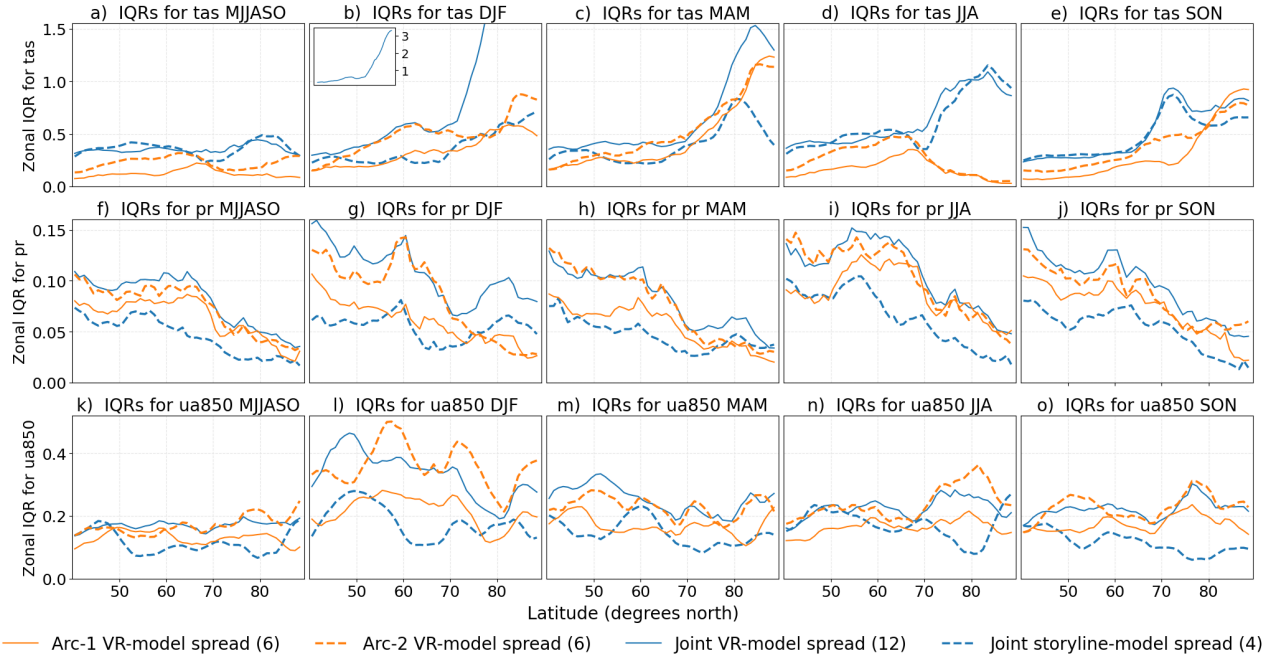

Figure S3. Zonal-mean interquartile ranges (IQRs) for near-surface temperature (tas; a–e), total precipitation rate (pr; f–j), and 850-hPa zonal wind (ua850; k–o) for the Arc-1 (solid orange line), Arc-2 (dashed orange line), and combined Arc-1 and Arc-2 (solid blue line) VR-model future responses (Arc-1/Arc-2 CESM/ICON/MPAS-UU/RU responses) and for the combined storyline-model responses for both time periods (CNRM/NorESM-10/30 responses; dashed blue lines). We show results for MJJASO (a, f, and k), DJF (b, g, and l), MAM (c, h, and m), JJA (d, i, and n), and SON (e, j, and o). The future responses are defined in Table S2. The number in parentheses in the legend indicates the number of future responses used. The inset in (b) shows the full range for the combined VR-model spread. The IQRs are computed for each grid point, excluding points without valid values for all responses, and subsequently zonally averaged. Note that the y-axis limits differ between rows. Units are K K^{-1} (a–e), mm day^{-1} K^{-1} (f–j), and m s^{-1} K^{-1} (k–o).

6 Plots for Antarctic storyline-model and VR-model experiments

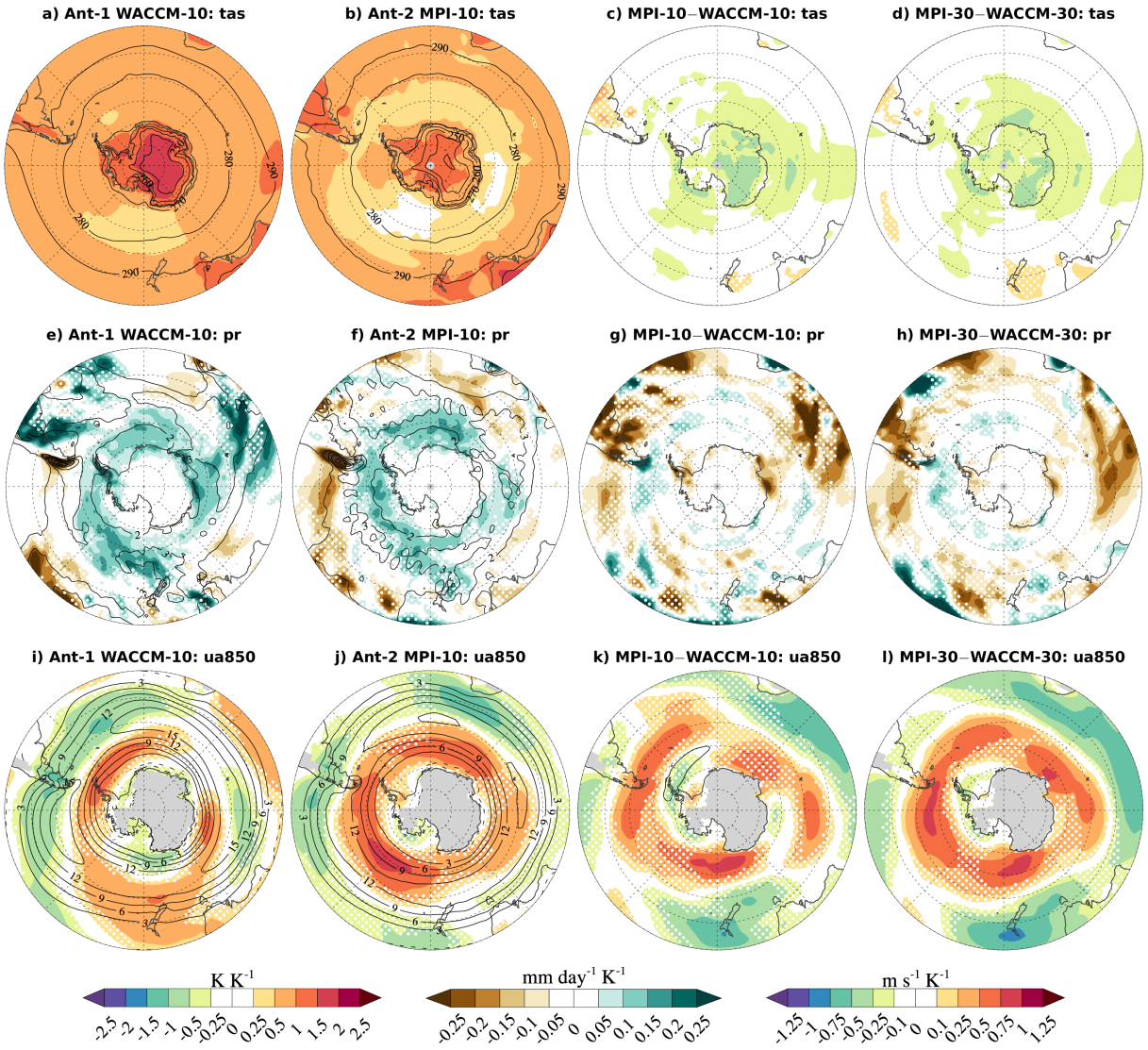

Figure S4. Future changes in near-surface temperature (tas; a–d), total precipitation rate (pr; e–h), and 850-hPa zonal wind (ua850; i–l) for the Antarctic storyline models during DJFM. We show the future response for Ant-1 WACCM-10 (a, e, and i) and Ant-2 MPI-10 (b, f, and j). To highlight the difference between the storyline models and assess the sensitivity to the time periods, we also show the difference between Ant-2 MPI-10 and Ant-1 WACCM-10 (c, g, and k), and between Ant-2 MPI-30 and Ant-1 WACCM-30 (d, h, and l). The future responses are defined in Table S3. Black contours, white dots and normalization is as in Fig. S2. Note that the responses in a–b are also shown in Fig. 8 in the main text, but are repeated here for convenience. Units of K K^{-1} (a–d), mm day^{-1} K^{-1} (d–h), and m s^{-1} K^{-1} (i–l).

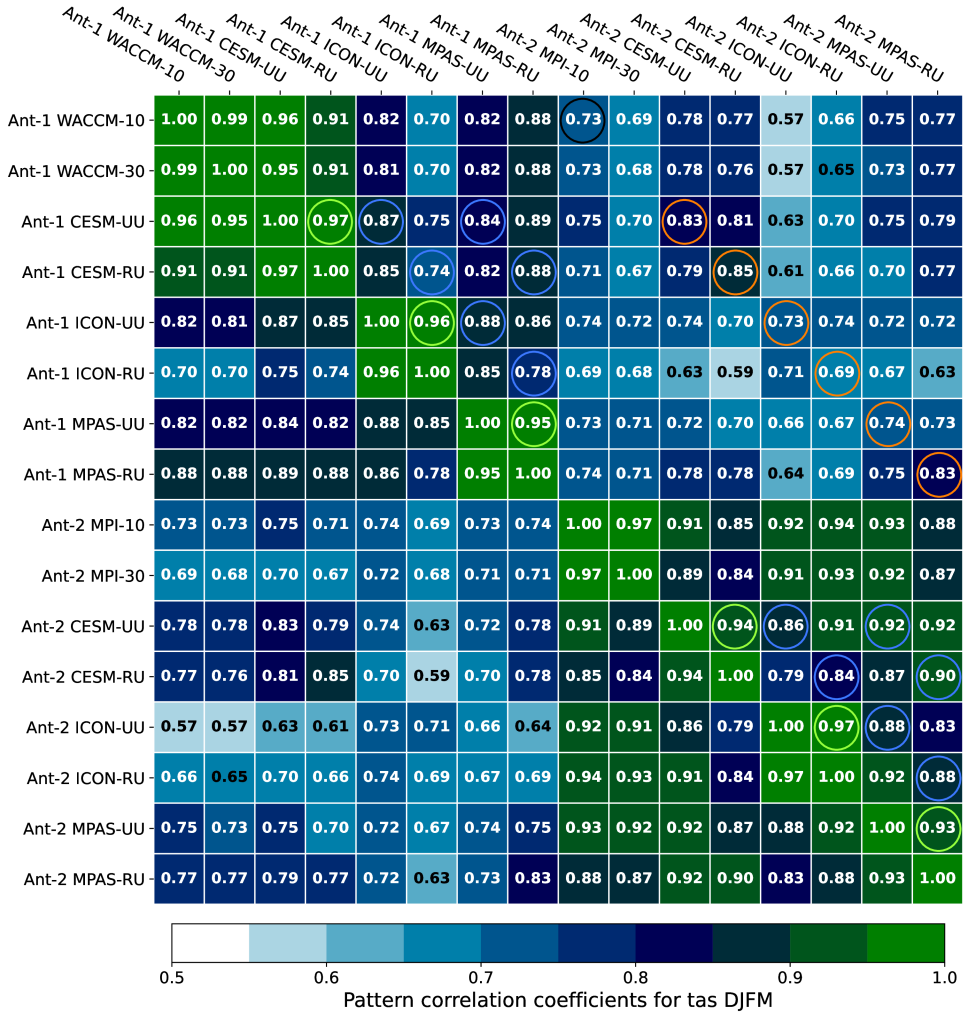

Figure S5. Pattern correlation matrix for future changes in near-surface temperature (tas) during DJFM for the Antarctic storyline models (Ant-1 WACCM-10/30 and Ant-2 MPI-10/30) and VR models (Ant-1/Ant-2 CESM/ICON/MPAS-UU/RU). Orange, blue, green, and black circles highlight the coefficients we use to estimate the storyline influence (equation 1 and 2 in the main text), VR-model influence (equation 1 and 3 in the main text), resolution influence (equation 1 and 4 in the main text), and the forcing-model contrast (equation 1 and 6 in the main text), respectively. Future responses are defined in Table S3. The correlation coefficients are computed for latitudes $\geq 30^{\circ}$S and cosine weighted. Units are dimensionless.

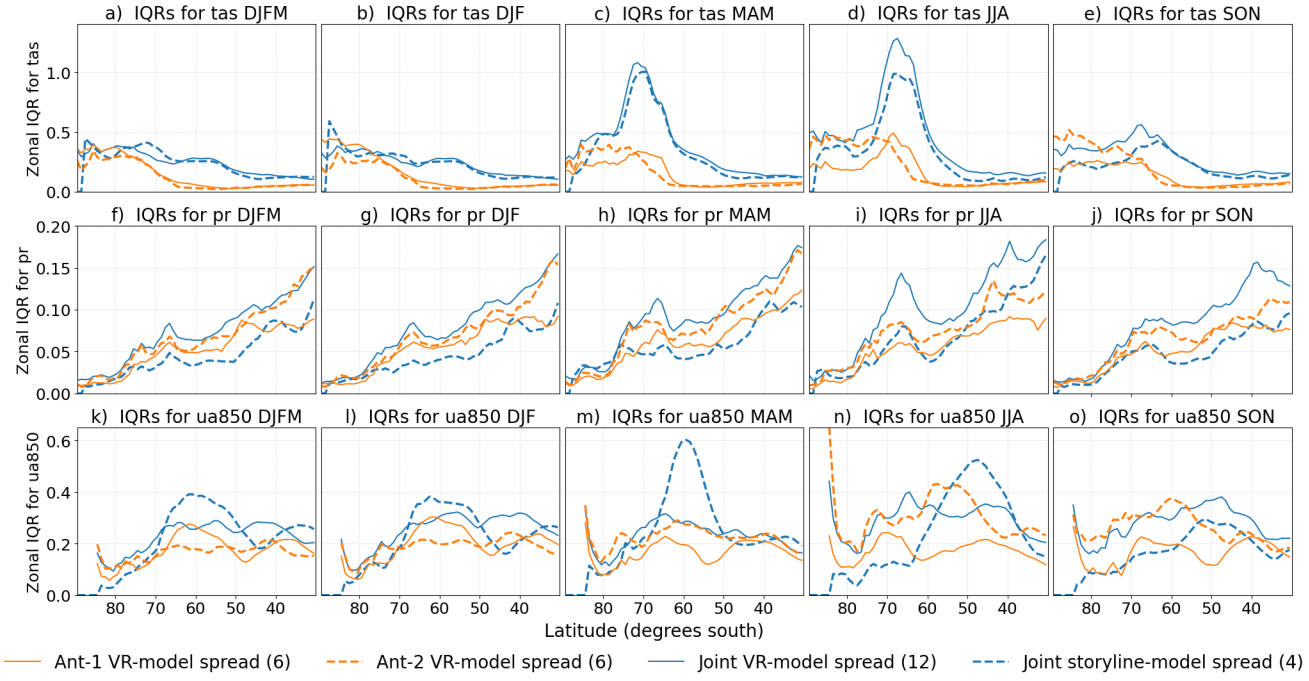

Figure S6. Zonal-mean interquartile ranges (IQRs) for near-surface temperature (tas; a–e), total precipitation rate (pr; f–j), and 850-hPa zonal wind (ua850; k–o) for the Ant-1 (solid orange line), Ant-2 (dashed orange line), and combined Ant-1 and Ant-2 (solid blue line) VR-model future responses (Ant-1/Ant-2 CESM/ICON/MPAS-UU/RU responses) and for the combined storyline-model responses for both time periods (Ant-1 WACCM-10/30 and Ant-2 MPI-10/30 responses; dashed blue lines). We show results for DJFM (a, f, and k), DJF (b, g, and l), MAM (c, h, and m), JJA (d, i, and n), and SON (e, j, and o). The future responses are defined in Table S3. The numbers in the legend and exclusion of grid points with non-values values is as in Fig. S3. Note that the y-axis limits differ between rows. Units are K K^{-1} (a–e), mm day^{-1} K^{-1} (f–j), and m s^{-1} K^{-1} (k–o).

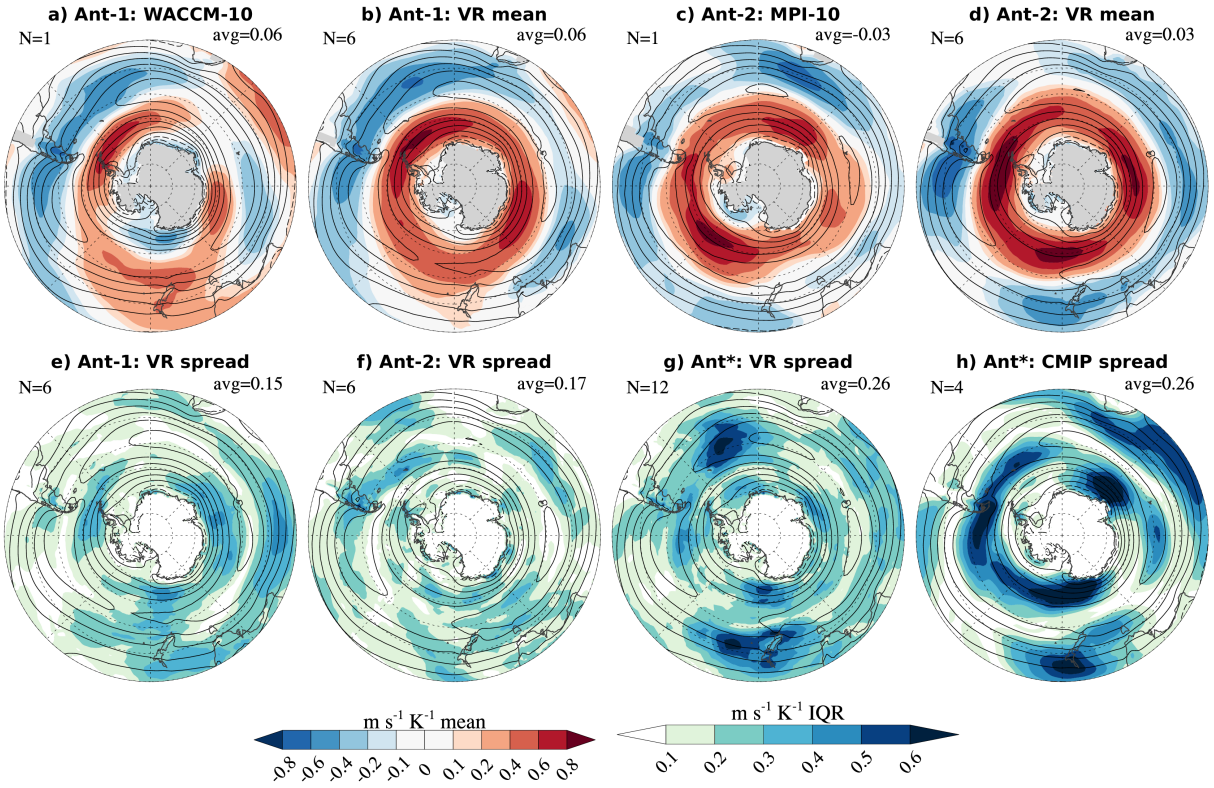

Figure S7. Future change in 850-hPa zonal wind during DJFM for the Ant-1 storyline model (WACCM-10; a), the Ant-2 VR-model mean (Ant-2 CESM/ICON/MPAS-UU/RU responses; b), the Ant-2 storyline model (MPI-10 response; c), and the Ant-2 VR-model mean (Ant-2 CESM/ICON/MPAS-UU/RU; d). Also shown is the interquartile range (spread) for the Ant-1 (e), Ant-2 (f), and combined Ant-1 and Ant-2 (g) VR-model responses (Ant-1/Ant-2, CESM/ICON/MPAS-UU/RR), and for the combined storyline-model responses for both time periods (WACCM-10/30 and MPI-10/30; h). N denotes the number of response fields in each panel. Future responses are defined in Table S3 and normalized by global near-surface warming. Units are m s^{-1} K^{-1}.

7 Precipitation summary metrics for the polar regions

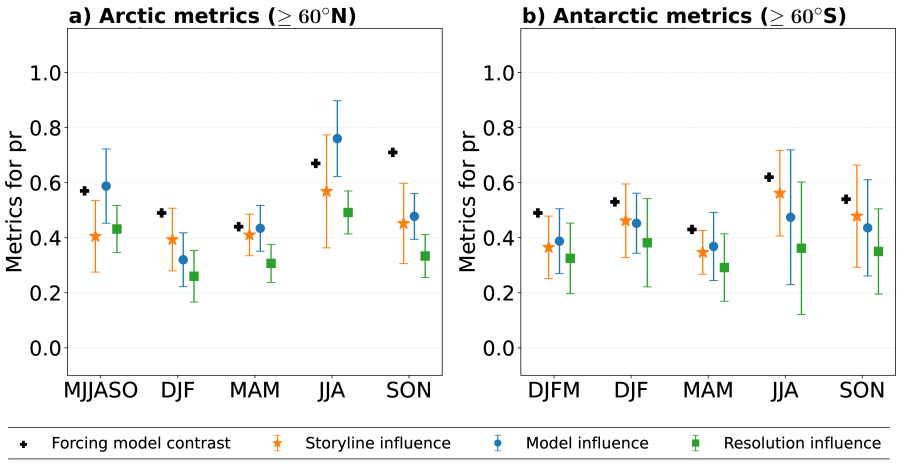

Figure S8. Summary metrics for precipitation for the polar regions for the Arctic storyline-model and VR-model experiments (a) and the antarctic storyline-model and VR-model experiments (b). Each panel shows the storyline influence (equation 1 and 2 in the main text; orange stars), VR-model influence (equation 1 and 3 in the main text; blue dots), resolution influence (equation 1 and 4 in the main text; green squares), and forcing-model contrast (equation 1 and 6 in the main text; black plus signs) for total precipitation rate (pr) for MJJASO (a) or DJFM (b), DJF, MAM, JJA, and SON. For the influence metrics, markers denote the mean and vertical bars $\pm$ one standard deviation (equation 7 in the main text). The forcing-model contrast is based on a single pattern correlation coefficient, and the marker shows this value. The correlation coefficients the metrics are based on are computed for latitudes $\geq 60^{\circ}$N in a and latitudes $\geq 60^{\circ}$S in b and are cosine weighted to account for varying grid-cell are with latitude. Units are dimensionless.

8 Comparison of CESM-RU and CESM-RR response patterns

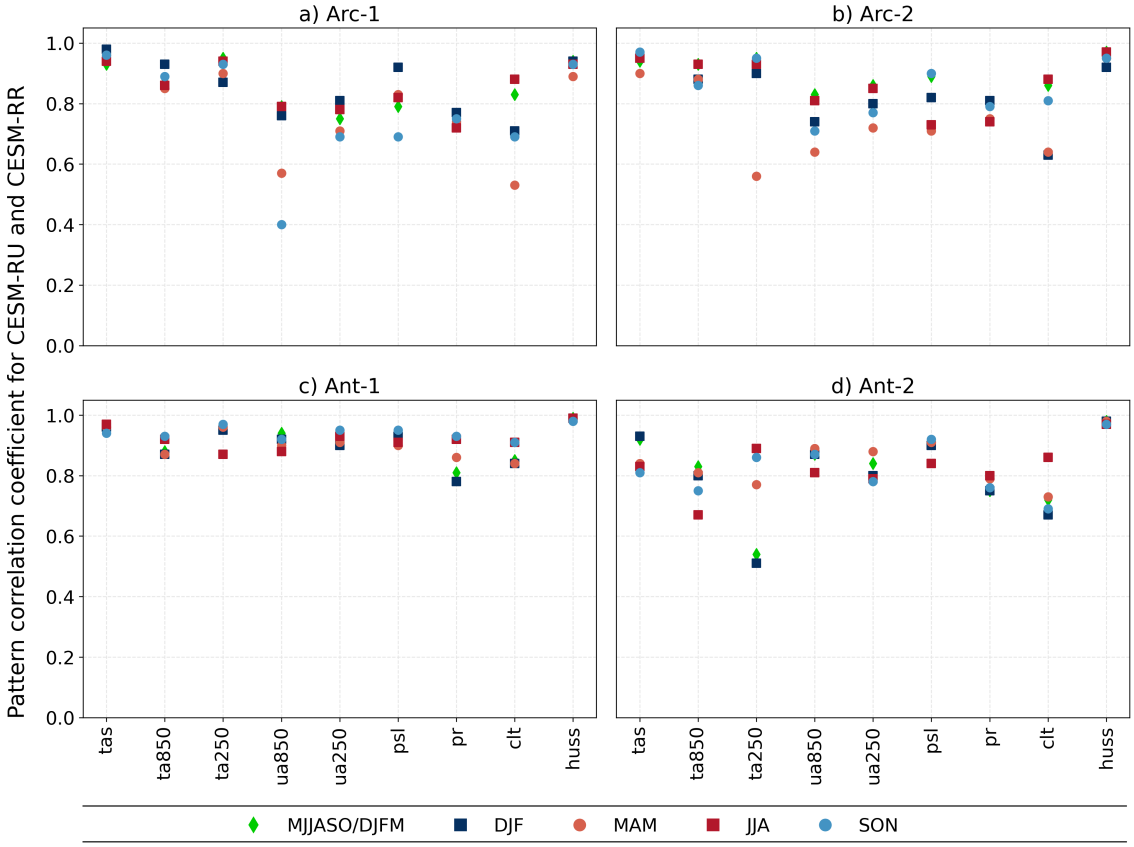

Figure S9. Pattern correlation coefficients between the CESM-RU and CESM-RR (future dual-polar refined−recent-past dual-polar refined) responses for near-surface, 850-hPa, and 250-hPa temperature (tas, ta850, and ta250; $K\ K^{-1}$), 850-hPa and 250-hPa zonal wind (ua850 and ua250; m s^{-1} K^{-1}), sea level pressure (psl; Pa K^{-1}), total precipitation rate (pr; mm day^{-1} K^{-1}), total cloud cover (clt; % K^{-1}), and near-surface specific humidity (huss; g kg^{-1} k^{-1}) for Arc-1 (a), Arc-2 (b), Ant-1 (c), and Ant-2 (d). Seasons are distinguished by colored markers: green diamonds denote MJJASO in a–b and DJFM in c–d, dark blue squares denote DJF, light red circles MAM, dark red squares JJA, and light blue circles SON. The Arc-1, Arc-2, Ant1, and Ant-2 CESM-RU responses are defined in Table S2–S3. The CESM-RR responses correspond to the CESM-RU responses, but use the refined recent-past experiment (available only for CESM) instead of the unrefined recent-past experiment. Normalization is as in Fig. S2. Units are dimensionless.

References

Bader, D. C., Leung, R., Taylor, M., and McCoy, R. B.: E3SM-Project E3SM1.1ECA model output prepared for CMIP6 CMIP historical, https://doi.org/10.22033/ESGF/CMIP6.11486, 2020a.

Bader, D. C., Leung, R., Taylor, M., and McCoy, R. B.: E3SM-Project E3SM1.1 model output prepared for CMIP6 ScenarioMIP ssp585, https://doi.org/10.22033/ESGF/CMIP6.15179, 2020b.

Boucher, O., Denvil, S., Levavasseur, G., Cozic, A., Caubel, A., Foujols, M.-A., Meurdesoif, Y., Cadule, P., Devilliers, M., Ghattas, J., Lebas, N., Lurton, T., Mellul, L., Musat, I., Mignot, J., and Cheruy, F.: IPSL IPSL-CM6A-LR model output prepared for CMIP6 CMIP historical, https://doi.org/10.22033/ESGF/CMIP6.5195, 2018.

Boucher, O., Denvil, S., Levavasseur, G., Cozic, A., Caubel, A., Foujols, M.-A., Meurdesoif, Y., Cadule, P., Devilliers, M., Dupont, E., and Lurton, T.: IPSL IPSL-CM6A-LR model output prepared for CMIP6 ScenarioMIP ssp585, https://doi.org/10.22033/ESGF/CMIP6.5271, 2019.

Cao, J.: NUIST NESMv3 model output prepared for CMIP6 ScenarioMIP ssp585, https://doi.org/10.22033/ESGF/CMIP6.8790, 2019.

Cao, J. and Wang, B.: NUIST NESMv3 model output prepared for CMIP6 CMIP historical, https://doi.org/10.22033/ESGF/CMIP6.8769, 2019.

Chai, Z.: CAS CAS-ESM1.0 model output prepared for CMIP6 CMIP historical, https://doi.org/10.22033/ESGF/CMIP6.3353, 2020.

Chinese Academy Of Sciences (CAS): CAS CAS-ESM1.0 model output prepared for CMIP6 ScenarioMIP ssp585, https://doi.org/10.22033/ESGF/CMIP6.3501, 2020.

Danabasoglu, G.: NCAR CESM2 model output prepared for CMIP6 CMIP historical, https://doi.org/10.22033/ESGF/CMIP6.7627, 2019a.

Danabasoglu, G.: NCAR CESM2 model output prepared for CMIP6 ScenarioMIP ssp585, https://doi.org/10.22033/ESGF/CMIP6.7768, 2019b.

Danabasoglu, G.: NCAR CESM2-WACCM model output prepared for CMIP6 CMIP historical, https://doi.org/10.22033/ESGF/CMIP6.10071, 2019c.

Danabasoglu, G.: NCAR CESM2-WACCM model output prepared for CMIP6 ScenarioMIP ssp585, https://doi.org/10.22033/ESGF/CMIP6.10115, 2019d.

Dix, M., Bi, D., Dobrohotoff, P., Fiedler, R., Harman, I., Law, R., Mackallah, C., Marsland, S., O'Farrell, S., Rashid, H., Srbinovsky, J., Sullivan, A., Trenham, C., Vohralik, P., Watterson, I., Williams, G., Woodhouse, M., Bodman, R., Dias, F. B., Domingues, C. M., Hannah, N., Heerdegen, A., Savita, A., Wales, S., Allen, C., Druken, K., Evans, B., Richards, C., Ridzwan, S. M., Roberts, D., Smillie, J., Snow, K., Ward, M., and Yang, R.: CSIRO-ARCCSS ACCESS-CM2 model output prepared for CMIP6 CMIP historical, https://doi.org/10.22033/ESGF/CMIP6.4271, 2019a.

Dix, M., Bi, D., Dobrohotoff, P., Fiedler, R., Harman, I., Law, R., Mackallah, C., Marsland, S., O'Farrell, S., Rashid, H., Srbinovsky, J., Sullivan, A., Trenham, C., Vohralik, P., Watterson, I., Williams, G., Woodhouse, M., Bodman, R., Dias, F. B., Domingues, C. M., Hannah, N., Heerdegen, A., Savita, A., Wales, S., Allen, C., Druken, K., Evans, B., Richards, C., Ridzwan, S. M., Roberts, D., Smillie, J., Snow, K., Ward, M., and Yang, R.: CSIRO-ARCCSS ACCESS-CM2 model output prepared for CMIP6 ScenarioMIP ssp585, https://doi.org/10.22033/ESGF/CMIP6.4332, 2019b.

EC-Earth Consortium (EC-Earth): EC-Earth-Consortium EC-Earth3-Veg model output prepared for CMIP6 CMIP historical, https://doi.org/10.22033/ESGF/CMIP6.4706, 2019a.

EC-Earth Consortium (EC-Earth): EC-Earth-Consortium EC-Earth3-Veg model output prepared for CMIP6 ScenarioMIP ssp585, https://doi.org/10.22033/ESGF/CMIP6.4914, 2019b.

EC-Earth Consortium (EC-Earth): EC-Earth-Consortium EC-Earth3 model output prepared for CMIP6 CMIP historical, https://doi.org/10.22033/ESGF/CMIP6.4700, 2019c.

EC-Earth Consortium (EC-Earth): EC-Earth-Consortium EC-Earth3 model output prepared for CMIP6 ScenarioMIP ssp585, https://doi.org/10.22033/ESGF/CMIP6.4912, 2019d.

EC-Earth Consortium (EC-Earth): EC-Earth-Consortium EC-Earth3-Veg-LR model output prepared for CMIP6 CMIP historical, https://doi.org/10.22033/ESGF/CMIP6.4707, 2020a.

EC-Earth Consortium (EC-Earth): EC-Earth-Consortium EC-Earth3-Veg-LR model output prepared for CMIP6 ScenarioMIP ssp585, https://doi.org/10.22033/ESGF/CMIP6.4915, 2020b.

EC-Earth Consortium (EC-Earth): EC-Earth-Consortium EC-Earth-3-CC model output prepared for CMIP6 CMIP historical, https://doi.org/10.22033/ESGF/CMIP6.4702, 2021a.

EC-Earth Consortium (EC-Earth): EC-Earth-Consortium EC-Earth3-CC model output prepared for CMIP6 ScenarioMIP ssp585, https://doi.org/10.22033/ESGF/CMIP6.15636, 2021b.

Good, P.: MOHC HadGEM3-GC31-LL model output prepared for CMIP6 ScenarioMIP ssp585, https://doi.org/10.22033/ESGF/CMIP6.10901, 2020.

Good, P., Sellar, A., Tang, Y., Rumbold, S., Ellis, R., Kelley, D., and Kuhlbrodt, T.: MOHC UKESM1.0-LL model output prepared for CMIP6 ScenarioMIP ssp585, https://doi.org/10.22033/ESGF/CMIP6.6405, 2019.

Guo, H., John, J. G., Blanton, C., McHugh, C., Nikonov, S., Radhakrishnan, A., Rand, K., Zadeh, N. T., Balaji, V., Durachta, J., Dupuis, C., Menzel, R., Robinson, T., Underwood, S., Vahlenkamp, H., Bushuk, M., Dunne, K. A., Dussin, R., Gauthier, P. P., Ginoux, P., Griffies, S. M., Hallberg, R., Harrison, M., Hurlin, W., Lin, P., Malyshev, S., Naik, V., Paulot, F., Paynter, D. J., Ploshay, J., Reichl, B. G., Schwarzkopf, D. M., Seman, C. J., Shao, A., Silvers, L., Wyman, B., Yan, X., Zeng, Y., Adcroft, A., Dunne, J. P., Held, I. M., Krasting, J. P., Horowitz, L. W., Milly, P., Shevliakova, E., Winton, M., Zhao, M., and Zhang, R.: NOAA-GFDL GFDL-CM4 model output historical, https://doi.org/10.22033/ESGF/CMIP6.8594, 2018a.

Guo, H., John, J. G., Blanton, C., McHugh, C., Nikonov, S., Radhakrishnan, A., Rand, K., Zadeh, N. T., Balaji, V., Durachta, J., Dupuis, C., Menzel, R., Robinson, T., Underwood, S., Vahlenkamp, H., Dunne, K. A., Gauthier, P. P., Ginoux, P., Griffies, S. M., Hallberg, R., Harrison, M., Hurlin, W., Lin, P., Malyshev, S., Naik, V., Paulot, F., Paynter, D. J., Ploshay, J., Schwarzkopf, D. M., Seman, C. J., Shao, A., Silvers, L., Wyman, B., Yan, X., Zeng, Y., Adcroft, A., Dunne, J. P., Held, I. M., Krasting, J. P., Horowitz, L. W., Milly, C., Shevliakova, E., Winton, M., Zhao, M., and Zhang, R.: NOAA-GFDL GFDL-CM4 model output prepared for CMIP6 ScenarioMIP ssp585, https://doi.org/10.22033/ESGF/CMIP6.9268, 2018b.

Huang, W.: THU CIESM model output prepared for CMIP6 CMIP historical, https://doi.org/10.22033/ESGF/CMIP6.8843, 2019.

Huang, W.: THU CIESM model output prepared for CMIP6 ScenarioMIP ssp585, https://doi.org/10.22033/ESGF/CMIP6.8863, 2020.

Jackson, L.: MOHC HadGEM3-GC31-MM model output prepared for CMIP6 ScenarioMIP ssp585, https://doi.org/10.22033/ESGF/CMIP6.10902, 2020.

John, J. G., Blanton, C., McHugh, C., Radhakrishnan, A., Rand, K., Vahlenkamp, H., Wilson, C., Zadeh, N. T., Dunne, J. P., Dussin, R., Horowitz, L. W., Krasting, J. P., Lin, P., Malyshev, S., Naik, V., Ploshay, J., Shevliakova, E., Silvers, L., Stock, C., Winton, M., and Zeng, Y.: NOAA-GFDL GFDL-ESM4 model output prepared for CMIP6 ScenarioMIP ssp585, https://doi.org/10.22033/ESGF/CMIP6.8706, 2018.

Jungclaus, J., Bittner, M., Wieners, K.-H., Wachsmann, F., Schupfner, M., Legutke, S., Giorgetta, M., Reick, C., Gayler, V., Haak, H., de Vrese, P., Raddatz, T., Esch, M., Mauritsen, T., von Storch, J.-S., Behrens, J., Brovkin, V., Claussen, M., Crueger, T., Fast, I., Fiedler, S., Hagemann, S., Hohenegger, C., Jahns, T., Kloster, S., Kinne, S., Lasslop, G., Kornblueh, L., Marotzke, J., Matei, D., Meraner, K., Mikolajewicz, U., Modali, K., Müller, W., Nabel, J., Notz, D., Peters-von Gehlen, K., Pincus, R., Pohlmann, H., Pongratz, J., Rast, S., Schmidt, H., Schnur, R., Schulzweida, U., Six, K., Stevens, B., Voigt, A., and Roeckner, E.: MPI-M MPI-ESM1.2-HR model output prepared for CMIP6 CMIP historical, https://doi.org/10.22033/ESGF/CMIP6.6594, 2019.

Kim, Y., Noh, Y., Kim, D., Lee, M.-I., Lee, H. J., Kim, S. Y., and Kim, D.: KIOST KIOST-ESM model output prepared for CMIP6 CMIP historical, https://doi.org/10.22033/ESGF/CMIP6.5296, 2019a.

Kim, Y., Noh, Y., Kim, D., Lee, M.-I., Lee, H. J., Kim, S. Y., and Kim, D.: KIOST KIOST-ESM model output prepared for CMIP6 ScenarioMIP ssp585, https://doi.org/10.22033/ESGF/CMIP6.11249, 2019b.

Krasting, J. P., John, J. G., Blanton, C., McHugh, C., Nikonov, S., Radhakrishnan, A., Rand, K., Zadeh, N. T., Balaji, V., Durachta, J., Dupuis, C., Menzel, R., Robinson, T., Underwood, S., Vahlenkamp, H., Dunne, K. A., Gauthier, P. P., Ginoux, P., Griffies, S. M., Hallberg, R., Harrison, M., Hurlin, W., Malyshev, S., Naik, V., Paulot, F., Paynter, D. J., Ploshay, J., Reichl, B. G., Schwarzkopf, D. M., Seman, C. J., Silvers, L., Wyman, B., Zeng, Y., Adcroft, A., Dunne, J. P., Dussin, R., Guo, H., He, J., Held, I. M., Horowitz, L. W., Lin, P., Milly, P., Shevliakova, E., Stock, C., Winton, M., Wittenberg, A. T., Xie, Y., and Zhao, M.: NOAA-GFDL GFDL-ESM4 model output prepared for CMIP6 CMIP historical, https://doi.org/10.22033/ESGF/CMIP6.8597, 2018.

Lovato, T. and Peano, D.: CMCC CMCC-CM2-SR5 model output prepared for CMIP6 ScenarioMIP ssp585, https://doi.org/10.22033/ESGF/CMIP6.3896, 2020a.

Lovato, T. and Peano, D.: CMCC CMCC-CM2-SR5 model output prepared for CMIP6 CMIP historical, https://doi.org/10.22033/ESGF/CMIP6.3825, 2020b.

Lovato, T., Peano, D., and Butenschön, M.: CMCC CMCC-ESM2 model output prepared for CMIP6 ScenarioMIP ssp585, https://doi.org/10.22033/ESGF/CMIP6.13259, 2021a.

Lovato, T., Peano, D., and Butenschön, M.: CMCC CMCC-ESM2 model output prepared for CMIP6 CMIP historical, https://doi.org/10.22033/ESGF/CMIP6.13195, 2021b.

NASA Goddard Institute For Space Studies (NASA/GISS): NASA-GISS GISS-E2.1G model output prepared for CMIP6 CMIP historical, https://doi.org/10.22033/ESGF/CMIP6.7127, 2018.

NASA Goddard Institute For Space Studies (NASA/GISS): NASA-GISS GISS-E2.1G model output prepared for CMIP6 ScenarioMIP ssp585, https://doi.org/10.22033/ESGF/CMIP6.7460, 2020.

Ridley, J., Menary, M., Kuhlbrodt, T., Andrews, M., and Andrews, T.: MOHC HadGEM3-GC31-LL model output prepared for CMIP6 CMIP historical, https://doi.org/10.22033/ESGF/CMIP6.6109, 2019a.

Ridley, J., Menary, M., Kuhlbrodt, T., Andrews, M., and Andrews, T.: MOHC HadGEM3-GC31-MM model output prepared for CMIP6 CMIP historical, https://doi.org/10.22033/ESGF/CMIP6.6112, 2019b.

Rong, X.: CAMS CAMS_CSM1.0 model output prepared for CMIP6 CMIP historical, https://doi.org/10.22033/ESGF/CMIP6.9754, 2019a.

Rong, X.: CAMS CAMS-CSM1.0 model output prepared for CMIP6 ScenarioMIP ssp585, https://doi.org/10.22033/ESGF/CMIP6.11052, 2019b.

Schupfner, M., Wieners, K.-H., Wachsmann, F., Steger, C., Bittner, M., Jungclaus, J., Früh, B., Pankatz, K., Giorgetta, M., Reick, C., Legutke, S., Esch, M., Gayler, V., Haak, H., de Vrese, P., Raddatz, T., Mauritsen, T., von Storch, J.-S., Behrens, J., Brovkin, V., Claussen, M., Crueger, T., Fast, I., Fiedler, S., Hagemann, S., Hohenegger, C., Jahns, T., Kloster, S., Kinne, S., Lasslop, G., Kornblueh, L., Marotzke, J., Matei, D., Meraner, K., Mikolajewicz, U., Modali, K., Müller, W., Nabel, J., Notz, D., Peters-von Gehlen, K., Pincus, R., Pohlmann, H., Pongratz, J., Rast, S., Schmidt, H., Schnur, R., Schulzweida, U., Six, K., Stevens, B., Voigt, A., and Roeckner, E.: DKRZ MPI-ESM1.2-HR model output prepared for CMIP6 ScenarioMIP ssp585, https://doi.org/10.22033/ESGF/CMIP6.4403, 2019.

Seferian, R.: CNRM-CERFACS CNRM-ESM2-1 model output prepared for CMIP6 CMIP historical, https://doi.org/10.22033/ESGF/CMIP6.4068, 2018.

Song, Z., Qiao, F., Bao, Y., Shu, Q., Song, Y., and Yang, X.: FIO-QLNM FIO-ESM2.0 model output prepared for CMIP6 CMIP historical, https://doi.org/10.22033/ESGF/CMIP6.9199, 2019a.

Song, Z., Qiao, F., Bao, Y., Shu, Q., Song, Y., and Yang, X.: FIO-QLNM FIO-ESM2.0 model output prepared for CMIP6 ScenarioMIP ssp585, https://doi.org/10.22033/ESGF/CMIP6.9214, 2019b.

Tang, Y., Rumbold, S., Ellis, R., Kelley, D., Mulcahy, J., Sellar, A., Walton, J., and Jones, C.: MOHC UKESM1.0-LL model output prepared for CMIP6 CMIP historical, https://doi.org/10.22033/ESGF/CMIP6.6113, 2019.

Voldoire, A.: CMIP6 simulations of the CNRM-CERFACS based on CNRM-CM6-1 model for CMIP experiment historical, https://doi.org/10.22033/ESGF/CMIP6.4066, 2018.

Voldoire, A.: CNRM-CERFACS CNRM-CM6-1-HR model output prepared for CMIP6 CMIP historical, https://doi.org/10.22033/ESGF/CMIP6.4067, 2019a.

Voldoire, A.: CNRM-CERFACS CNRM-CM6-1-HR model output prepared for CMIP6 ScenarioMIP ssp585, https://doi.org/10.22033/ESGF/CMIP6.4225, 2019b.

Voldoire, A.: CNRM-CERFACS CNRM-CM6-1 model output prepared for CMIP6 ScenarioMIP ssp585, https://doi.org/10.22033/ESGF/CMIP6.4224, 2019c.

Voldoire, A.: CNRM-CERFACS CNRM-ESM2-1 model output prepared for CMIP6 ScenarioMIP ssp585, https://doi.org/10.22033/ESGF/CMIP6.4226, 2019d.

Volodin, E., Mortikov, E., Gritsun, A., Lykossov, V., Galin, V., Diansky, N., Gusev, A., Kostrykin, S., Iakovlev, N., Shestakova, A., and Emelina, S.: INM INM-CM5-0 model output prepared for CMIP6 CMIP historical, https://doi.org/10.22033/ESGF/CMIP6.5070, 2019a.

Volodin, E., Mortikov, E., Gritsun, A., Lykossov, V., Galin, V., Diansky, N., Gusev, A., Kostrykin, S., Iakovlev, N., Shestakova, A., and Emelina, S.: INM INM-CM5-0 model output prepared for CMIP6 ScenarioMIP ssp585, https://doi.org/10.22033/ESGF/CMIP6.12338, 2019b.

Wieners, K.-H., Giorgetta, M., Jungclaus, J., Reick, C., Esch, M., Bittner, M., Gayler, V., Haak, H., de Vrese, P., Raddatz, T., Mauritsen, T., von Storch, J.-S., Behrens, J., Brovkin, V., Claussen, M., Crueger, T., Fast, I., Fiedler, S., Hagemann, S., Hohenegger, C., Jahns, T., Kloster, S., Kinne, S., Lasslop, G., Kornblueh, L., Marotzke, J., Matei, D., Meraner, K., Mikolajewicz, U., Modali, K., Müller, W., Nabel, J., Notz, D., Peters-von Gehlen, K., Pincus, R., Pohlmann, H., Pongratz, J., Rast, S., Schmidt, H., Schnur, R., Schulzweida, U., Six, K., Stevens, B., Voigt, A., and Roeckner, E.: MPI-M MPI-ESM1.2-LR model output prepared for CMIP6 ScenarioMIP ssp585, https://doi.org/10.22033/ESGF/CMIP6.6705, 2019a.

Wieners, K.-H., Giorgetta, M., Jungclaus, J., Reick, C., Esch, M., Bittner, M., Legutke, S., Schupfner, M., Wachsmann, F., Gayler, V., Haak, H., de Vrese, P., Raddatz, T., Mauritsen, T., von Storch, J.-S., Behrens, J., Brovkin, V., Claussen, M., Crueger, T., Fast, I., Fiedler, S., Hagemann, S., Hohenegger, C., Jahns, T., Kloster, S., Kinne, S., Lasslop, G., Kornblueh, L., Marotzke, J., Matei, D., Meraner, K., Mikolajewicz, U., Modali, K., Müller, W., Nabel, J., Notz, D., Peters-von Gehlen, K., Pincus, R., Pohlmann, H., Pongratz, J., Rast, S., Schmidt, H., Schnur, R., Schulzweida, U., Six, K., Stevens, B., Voigt, A., and Roeckner, E.: MPI-M MPI-ESM1.2-LR model output prepared for CMIP6 CMIP historical, https://doi.org/10.22033/ESGF/CMIP6.6595, 2019b.

Williams, R. S., Marshall, G. J., Levine, X., Graff, L. S., Handorf, D., Johnston, N. M., Karpechko, A. Y., Orr, A., Van de Berg, W. J., Wijngaard, R. R., and Mooney, P. A.: Future Antarctic Climate: Storylines of Midlatitude Jet Strengthening and Shift Emergent from CMIP6, Journal of Climate, 37, 2157–2178, https://doi.org/10.1175/jcli-d-23-0122.1, 2024.

Wu, T., Chu, M., Dong, M., Fang, Y., Jie, W., Li, J., Li, W., Liu, Q., Shi, X., Xin, X., Yan, J., Zhang, F., Zhang, J., Zhang, L., and Zhang, Y.: BCC BCC-CSM2MR model output prepared for CMIP6 CMIP historical, https://doi.org/10.22033/ESGF/CMIP6.2948, 2018.

Xin, X., Wu, T., Shi, X., Zhang, F., Li, J., Chu, M., Liu, Q., Yan, J., Ma, Q., and Wei, M.: BCC BCC-CSM2MR model output prepared for CMIP6 ScenarioMIP ssp585, https://doi.org/10.22033/ESGF/CMIP6.3050, 2019.

Yukimoto, S., Koshiro, T., Kawai, H., Oshima, N., Yoshida, K., Urakawa, S., Tsujino, H., Deushi, M., Tanaka, T., Hosaka, M., Yoshimura, H., Shindo, E., Mizuta, R., Ishii, M., Obata, A., and Adachi, Y.: MRI MRI-ESM2.0 model output prepared for CMIP6 CMIP historical, https://doi.org/10.22033/ESGF/CMIP6.6842, 2019a.

Yukimoto, S., Koshiro, T., Kawai, H., Oshima, N., Yoshida, K., Urakawa, S., Tsujino, H., Deushi, M., Tanaka, T., Hosaka, M., Yoshimura, H., Shindo, E., Mizuta, R., Ishii, M., Obata, A., and Adachi, Y.: MRI MRI-ESM2.0 model output prepared for CMIP6 ScenarioMIP ssp585, https://doi.org/10.22033/ESGF/CMIP6.6929, 2019b.

Ziehn, T., Chamberlain, M., Lenton, A., Law, R., Bodman, R., Dix, M., Wang, Y., Dobrohotoff, P., Srbinovsky, J., Stevens, L., Vohralik, P., Mackallah, C., Sullivan, A., O'Farrell, S., and Druken, K.: CSIRO ACCESS-ESM1.5 model output prepared for CMIP6 ScenarioMIP ssp585, https://doi.org/10.22033/ESGF/CMIP6.4333, 2019a.

Ziehn, T., Chamberlain, M., Lenton, A., Law, R., Bodman, R., Dix, M., Wang, Y., Dobrohotoff, P., Srbinovsky, J., Stevens, L., Vohralik, P., Mackallah, C., Sullivan, A., O'Farrell, S., and Druken, K.: CSIRO ACCESS-ESM1.5 model output prepared for CMIP6 CMIP historical, https://doi.org/10.22033/ESGF/CMIP6.4272, 2019b.